Understanding the Role of Oxygen in the Segregation of Sodium at the Surface of Molybdenum Coated Soda-Lime Glass

Robert V. Forest
Dept. of Chemical and Biomolecular Engineering, University of Delaware, Newark, DE 19716

Institute of Energy Conversion, University of Delaware, Newark, DE 19716

Erten Eser, Brian E. McCandless, and Robert W. Birkmire
Institute of Energy Conversion, University of Delaware, Newark, DE 19716

Jingguang G. Chen
Dept. of Chemical Engineering, Columbia University, New York, NY 10027

DOI 10.1002/aic.14425
Published online March 11, 2014 in Wiley Online Library (wileyonlinelibrary.com)

Molybdenum (Mo) coated soda-lime glass is a commonly used substrate for Cu(InGa)Se_2 solar cells as it also acts as the sodium (Na) source, which improves the efficiency of these devices. In this work, we investigate how oxygen controls the segregation and accumulation of Na on the Mo surface. A direct relationship between the concentration of surface oxygen and the amount of Na accumulation is showed. Values for the surface segregation ratio and grain boundary diffusion coefficient for Na in Mo are obtained by fitting diffusion data at several temperatures to a model for grain boundary diffusion. The results of this model reveal that surface oxygen controls the Na saturation level through its effect on the surface segregation of Na. An activation energy for grain boundary diffusion of Na is estimated and is similar to that of Mo—O bond dissociation in MoO_3 suggesting the involvement of this bond during Na transport. © 2014 American Institute of Chemical Engineers *AIChE J*, 60: 2365–2372, 2014
Keywords: solar energy, grain boundary diffusion, Cu(InGa)Se_2, x-ray photoelectron spectroscopy

Introduction

With efficiencies exceeding 20%[1–3] and relatively low costs, Cu(InGa)Se_2 (CIGS) based photovoltaics remain a promising technology for realizing a \$0.50/watt manufacturing goal. To achieve higher efficiencies in CIGS devices, a small amount of sodium (Na) is incorporated into the CIGS film to improve open-circuit voltage (V_{OC}) and fill factor (FF) of the device.[4–6] Na can be incorporated from a variety of sources before, during, or after depositing the CIGS film.[7–12] One of the simplest methods is to allow Na to diffuse from a soda-lime glass (SLG) substrate through a thin molybdenum (Mo) layer during the CIGS deposition, where the Mo serves as an electrical contact to the back of the CIGS film. The high temperatures during deposition, typically greater than 450°C, cause Na to diffuse through the Mo and into the CIGS. The amount of Na incorporated using this approach is not well controlled and can result in nonuniform amounts of Na over large areas.[13] However, it remains an attractive option due to its simplicity and low cost. Developing a better understanding of the Na diffusion mechanism through Mo can potentially lead to solutions that overcome these controllability issues.

Although there have been several studies on how the Mo back contact affects Na incorporation in CIGS,[14–20] the specific diffusion mechanism is still not well understood. The current understanding is that at CIGS deposition temperatures, which range from 450 to 600°C, Na is highly mobile along Mo grain boundaries[14] but does not diffuse into the grain interiors since the solubility of Na is negligible up to at least 2623°C,[21] the melting point of Mo. Therefore, it is unlikely that any bulk transport takes place within the grain interiors of Mo. Because grains in a typical Mo back contact are columnar and span the entire height of the film,[22] the grain boundaries provide a fast diffusion path to the CIGS interface. Near the Mo/CIGS interface, Na tends to segregate, and this effect has been measured by different groups using secondary ion mass spectroscopy (SIMS).[15,16] The amount of Na that accumulates at the Mo surface may determine how much Na is incorporated into the rest of the CIGS film.[16]

The Mo void fraction or porosity has a large effect on the amount of Na incorporated into CIGS,[16–20] and less Na is observed in films grown on dense Mo compared to those grown on porous Mo.[16–19] It is believed that these voids

Additional Supporting Information may be found in the online version of this article.

Correspondence concerning this article should be addressed to R. W. Birkmire at rwb@udel.edu.

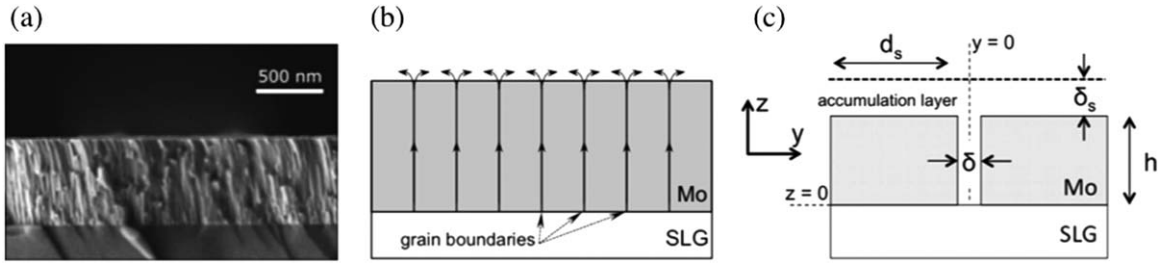

Figure 1. (a) Cross-section SEM image of sputter deposited Mo on SLG.

(b) Enlarged schematic of seven Mo grains with arrows denoting the diffusion path of Na. (c) Schematic depicting two adjacent Mo grains with their shared grain boundary. Dimensions used for diffusion modeling are depicted and are not shown to scale.

occur along grain boundaries and store oxygen, which is known to facilitate Na diffusion because of the strong affinity of Na for O_2.[14,16] Previous work in our group has shown that Na does not accumulate on the Mo surface when heating under high vacuum in the absence of oxygen.[23] CIGS deposited on intentionally oxidized Mo has been shown to have a higher Na concentration,[16] and CIGS devices made on intentionally oxidized Mo films show a small improvement in V_{OC} and FF, likely due to increased incorporation of Na.[24]

In this study, we evaluate the role that oxygen plays on the accumulation of Na on the Mo film surface. Specifically, we show that at a given temperature less Na accumulates on the Mo surface if oxygen is removed prior to Na diffusion and more accumulates if oxygen is added. Based on the experimental results, a diffusion model is used to explain Na diffusion from SLG and its accumulation on Mo. By fitting the model to diffusion data at different temperatures, the apparent activation energy for grain boundary diffusion of Na through Mo is determined.

Experimental Methods

Single layer Mo films were deposited using DC magnetron sputtering in 0.24 Pa of argon onto 2.5 × 2.5 cm^2 SLG substrates rotating at five revolutions per minutes. The sputter current was held at 1.5 A for 75 min resulting in ~700 nm thick films.

Surface compositions were measured using a PHI 5600 x-ray photoelectron spectrometer (XPS). The system was equipped with an aluminum anode x-ray source and a multichannel hemispherical analyzer. The binding energy scale was calibrated by comparing the position of primary photoelectron peaks from copper, silver, and gold reference foils to published values. Relative sensitivity factors (RSFs) for O and Mo were verified using MoO_3 powder, and the RSF for Na was verified using trisodium citrate ($Na_3C_6H_6O_7$).

The XPS chamber was equipped with a differentially pumped ion gun for sputter cleaning. An accelerating voltage of 2 kV, an emission current of 25 mA, and an argon pressure of 1.1×10^{-2} Pa were used, resulting in a sputter current of approximately 3 μA at the sample surface and a sputter rate of roughly 0.5 nm/min. The ion beam raster size was 1 × 1 cm^2, which covered the entire sample.

Sample heating was performed in a separate process chamber attached to the XPS system through a gate valve. Samples could be transferred between the process chamber and the XPS analysis chamber under vacuum and without exposure to ambient air. In the process chamber, a resistive heater of Ta wire was located 5 mm above the sample. Temperature was measured using an identical Mo/SLG reference sample with a K-type thermocouple permanently attached. The sample of interest is assumed to have the same temperature as the reference sample because they are both located at the same distance away from the heater. This setup allows the sample of interest to freely move between the process and analysis chambers without restriction from an attached thermocouple.

Results and Discussion

Characterization of Mo films

Cross-sectional scanning electron microscope (SEM) images were used to characterize the grain structure of the Mo films, and the measured dimensions will be used as input parameters when modeling the diffusion of Na through Mo. Figure 1a shows an SEM image of a Mo film that is 680 nm thick having columnar grains with an average width of 50 nm extending through the entire thickness of the film. Figure 1b shows a simplified cross-sectional schematic of the Mo film with arrows denoting the diffusion path of Na. Figure 1c shows a schematic of a close up of a Mo grain boundary along with adjacent grains and denotes the dimensions that will be used in modeling the diffusion of Na. Notation from this figure is discussed in the Diffusion Modeling section.

XPS scans of the Mo 3d, O 1s, and Na 1s regions were taken of the Mo/SLG surface and the composition was calculated from the peak areas divided by their RSF. The RSF adjusted peak area of an element was divided by the sum of the adjusted peak areas of all elements present to give an atomic percentage. Surface carbon was not included in this calculation.

Scans of the as-deposited Mo surface show 47 at % Mo and 53 at % O with no Na. The Mo 3d XPS spectrum shown in Figure 2a reveals that MoO_2, MoO_3, and metallic Mo are all present on the surface. For this particular sample, 82% of the Mo 3d region is metallic, 3% is MoO_2, and 15% is MoO_3. These peak areas of the Mo oxides are in good agreement with the actual percentage of oxygen measured. XPS depth profiling (Supporting Information Figure S1) reveals that MoO_3 exists only with the first few nanometers of the film, and only MoO_2 is detectable further in the film. Qualitative SIMS measurements (Supporting Information Figure S2) show that the oxygen level is nearly constant through the entire film and depth profiling with Auger electron spectroscopy (AES) reveals that the oxygen concentration within the Mo film is about 2 at %. Oxygen impurities in sputtered Mo films have been shown to originate from the residual gas in the sputter chamber.[25,26] Given the very low solubility of O in Mo,[27] most of this O must reside at grain boundaries.

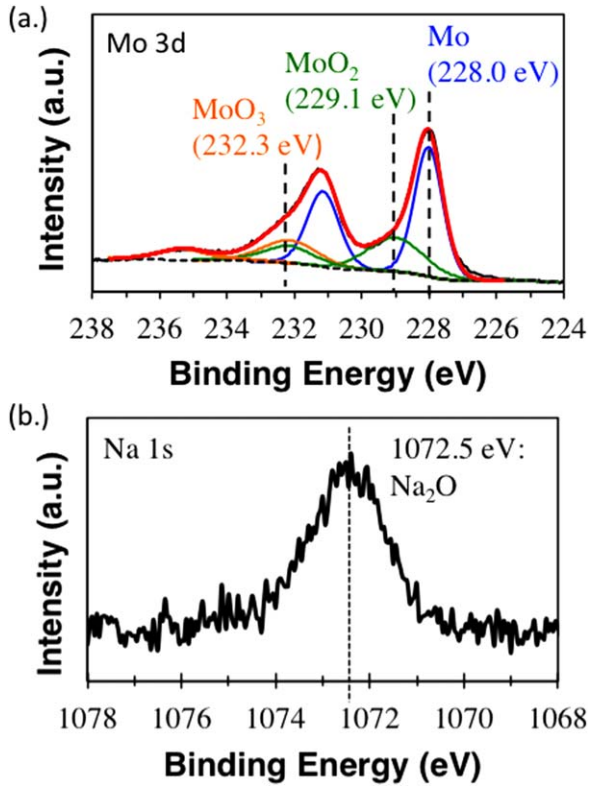

Figure 2. (a) XPS spectrum of Mo 3d region for as-deposited Mo surface with peaks for oxide and metallic species.

(b) XPS spectrum of Na 1s region for SLG/Mo sample after heating at 400°C for 10 min. [Color figure can be viewed in the online issue, which is available at wileyonlinelibrary.com.]

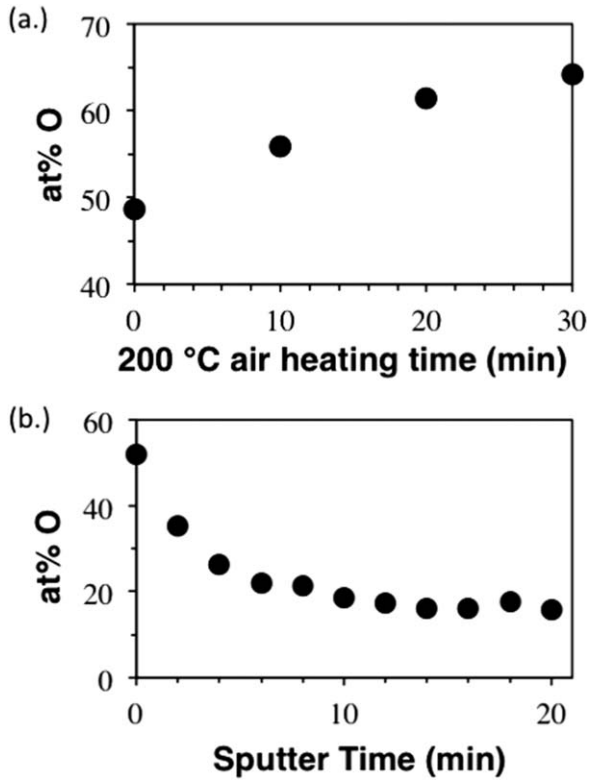

Figure 3. Surface oxygen content of Mo on SLG as measured by XPS for samples (a) heated in ambient air at 200°C and (b) sputtered in vacuum.

After heating the sample from Figure 2a for 10 min at 400°C, Na appears with a concentration of 4 at %. The Na 1s peak was located at 1072.5 eV as shown in Figure 2b, which is in agreement with the binding energy of Na_2O.

Controlling surface oxygen on Mo

To evaluate the relationship between the amount of oxygen on the Mo surface and the amount of Na accumulation, the concentration of surface oxygen was precisely controlled before diffusion experiments. The amount of oxygen on the surface of Mo was controlled by either sputtering to remove oxygen or heating in air to add oxygen.

Heat treating in ambient air at 200°C for 30 min increased the surface oxygen content from roughly 50 at % for the as-deposited sample to 65 at %, and Figure 3a shows the increase in surface oxygen as measured by XPS as a function of heat treatment time. Depth profiling measurements with XPS reveal that this oxide layer is only a few nanometers thick. It was determined that Na diffusion in Mo at this temperature is too slow to cause any significant diffusion of Na out of the glass during this heat treatment.

To remove oxygen from the Mo surface, samples were sputter etched inside the XPS analysis chamber at a sputtering rate of approximately 0.5 nm/min, and Figure 3b shows the decrease in surface oxygen with sputter time. The Mo thickness is reduced by less than 1% during sputtering, which will not significantly skew results from diffusion measurements. The oxygen concentration stabilizes at an artificially high concentration after long periods of etching, and it is most likely that a small amount of surface oxygen is pushed into the film during sputtering preventing the complete removal of oxygen from the surface. Surface oxygen concentrations as low as 16 at % can be achieved using this procedure. Diffusion experiments were performed immediately after etching and without exposure to ambient air to prevent reoxidation of the Mo surface.

Relationship of surface oxygen to Na segregation

The accumulation of Na on SLG/Mo during heating in vacuum was compared between a sample having 54 at % oxygen due to ambient air exposure, and a sample that had been sputter etched for 20 min to have 13 at % oxygen. These samples were heated in a vacuum of 10^{-5} Pa at 400°C for 1–2 min, cooled to near ambient temperature, then transferred to the XPS analysis chamber to measure the Na content. This process was repeated on the same sample until the concentration of Na stopped increasing. Figure 4 shows results of this experiment for both samples. Within 10 min of heating, the surface of both samples becomes saturated with Na, and the concentration no longer increases. The saturation concentration varies by nearly an order of magnitude between the low and high oxygen samples, suggesting that oxygen on the surface of Mo may affect the amount of Na that accumulates.

To clarify the relationship between surface oxygen and Na accumulation, similar heat treatments were performed where the oxygen concentration on SLG/Mo samples was varied from 27 to 59 at % using the techniques described above. These samples were heated under vacuum at either 400 or

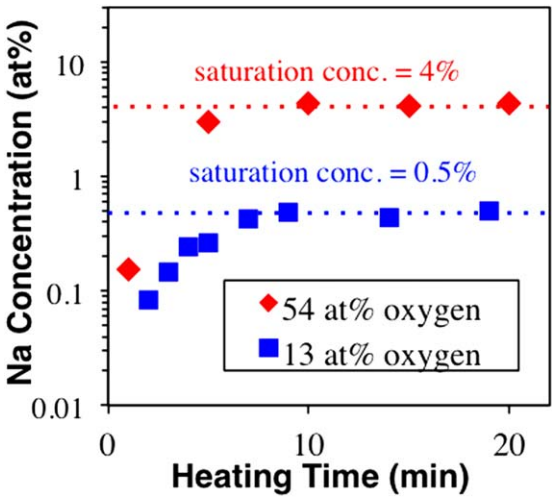

Figure 4. Na concentration on Mo surface as measured by XPS as a function of heating time at 400°C for samples with a high amount of surface oxygen (red diamonds) and low amount of surface oxygen (blue squares).

[Color figure can be viewed in the online issue, which is available at wileyonlinelibrary.com.]

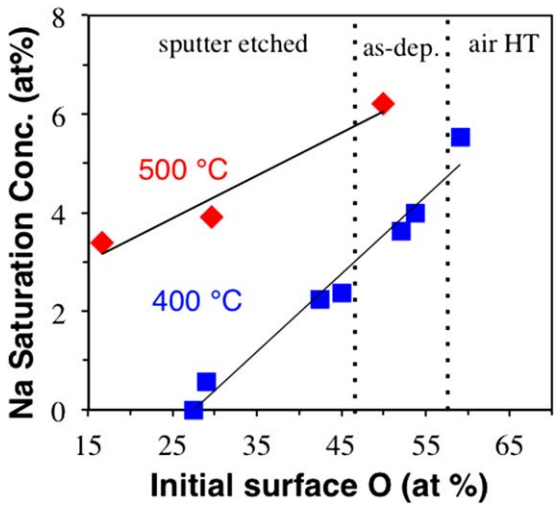

Figure 5. The saturation concentration of Na as a function of initial surface oxygen on the Mo film after heating in vacuum at 400°C (blue squares) or 500°C (red diamonds).

Surface oxygen was varied from as-deposited films by either sputter etching or heating in air at 200°C. [Color figure can be viewed in the online issue, which is available at wileyonlinelibrary.com.]

500°C until the Na concentration stopped increasing. In Figure 5, the saturation concentration is plotted against the amount of surface oxygen before heating. There is a linear relationship at both temperatures where samples with more surface oxygen accumulate more Na, which clearly demonstrates that surface oxygen plays a critical role in controlling the Na saturation concentration. At this point, it is not clear why the saturation concentration is greater for samples that were heated to higher temperatures. Mathematical modeling was then performed to explain the observed relationships and quantify the diffusion process.

Diffusion modeling

The accumulation of Na on the surface of Mo was modeled according to Harrison's type C diffusion regime where the grain boundary diffusion coefficient is much larger than the bulk lattice diffusion coefficient ($D_b >> D_l$). In this case, transport only takes place along grain boundaries and on the free surface while diffusion through grain interior is negligible. Such diffusion behavior is usually observed at temperatures below 35% of the melting point.[28] Therefore, this analysis is appropriate for this system due to the high melting point of Mo at 2623°C and the relatively low temperature range of 300–500°C used in this study.

To obtain a mathematical solution, an analysis is adopted from the two-dimensional model of Hwang and Balluffi describing type C diffusion through a thin film.[29] This analysis is performed for a single grain and can be extended to multigrained structures due to the symmetry of the microstructure. Figure 1c shows a schematic of a single grain boundary and adjacent grains along with several parameters used in this model. Based on the previously discussed SEM cross-sectional images, Mo grains were approximated as evenly spaced, parallel square columns with the grain width (d_s) and the film thickness (h) having values of 50 and 680 nm, respectively. Based on transmission electron microscopy measurements of Mo films performed by other groups, a value of 3 nm was used for the grain boundary width (δ).[30]

Lastly, the accumulation of Na is confined on the surface within a layer of fixed thickness δ_s. This fixed accumulation layer thickness is well justified since after the Na reaches its saturation concentration the Mo film is always detected by XPS, showing that accumulation does not continue indefinitely. It is assumed that the accumulation of Na is limited to a single monolayer, which gives δ_s a value of 0.2 nm. Although this is a somewhat arbitrary assumption, if diffusion does not occur in a perfect monolayer it should not significantly alter the estimation of the diffusion coefficient.[31]

The analysis begins by assuming all Na transport takes place according to Fick's second law. The generalized form for this is

$$\frac{\partial c(y,z,\ t)}{\partial t} = D(y,z)\nabla^2 c(y,z,t) \tag{1}$$

where c is the concentration of Na and D is the diffusion coefficient. z is defined as the direction parallel to the grain boundaries, and y is the direction perpendicular.

Because diffusion only takes place along grain boundaries and on the surface, the expression can be separated into two equations. The first equation accounts for diffusion along grain boundaries and the second accounts for diffusion across the surface

$$\frac{\partial c_b(z,\ t)}{\partial t} = D_b \frac{\partial^2 c_b(z,\ t)}{\partial z^2} \quad \text{for } 0 \le z \le h \tag{2}$$

$$\frac{\partial c_s(y,\ t)}{\partial t} = D_s \frac{\partial^2 c_s(y,\ t)}{\partial y^2} \quad \text{for } 0 \le y \le \frac{d_s}{2} \tag{3}$$

where c_b is the Na concentration along the grain boundaries, D_b is the grain boundary diffusion coefficient, c_s is the concentration of Na along the surface, and D_s is the surface diffusion coefficient.

To fully constrain both of these partial differential equations, four boundary conditions and two initial conditions are needed. The two initial conditions arise because the grain

boundary and surface are both free of Na at the start of heating

$$c_b(z,\ 0)=c_s(y,\ 0)=0 \text{ with } z \neq 0 \tag{4}$$

Because the amount of Na available from the glass greatly exceeds the total grain boundary and accumulation volume, a constant uniform Na concentration is assumed at the SLG/Mo interface. This can be expressed as the following boundary condition

$$c_b(0,\ t)=c_0 \tag{5}$$

where c_0 is the Na concentration within the SLG and at the SLG/Mo interface. This value is independent of position in y and does not vary with time. c_0 was determined from XPS measurements on bare SLG giving a value of 4 at % both before and after heating to 500°C for 10 min. This Na concentration is lower than expected for SLG and it is likely that near the surface the glass is Na poor.

The next two boundary conditions describe the transition of Na out of the grain boundaries and onto the Mo surface. The first condition accounts for the conservation of matter. The amount of Na leaving the grain boundary must equal the amount entering the surface

$$\delta D_b \frac{\partial c_b}{\partial z}\bigg|_{z=h} = 2\delta_s D_s \frac{\partial c_s}{\partial y}\bigg|_{y=0} \tag{6}$$

where δ_s is the thickness of the accumulation layer. The next boundary condition describes the segregation of Na between the grain boundaries and accumulation at the surface. It is assumed that a thermodynamic equilibrium can be maintained at this junction so that the concentration of Na is not necessarily continuous at the grain boundary exit, and that the amount of segregation is independent of concentration giving the following expression

$$c_b s' = c_s \text{ at } y=0 \text{ with } z=h \tag{7}$$

where s' is the surface segregation factor. This accounts for any discontinuity in the Na concentration due to surface segregation at the grain boundary exit. As s' approaches 1, segregation disappears and concentration becomes a continuous function during the transition to surface diffusion.

Finally, due to symmetry, the following condition on the sample surface must be met

$$\frac{\partial c_s}{\partial y}=0 \quad \text{at } y=d_s/2 \tag{8}$$

The full analytical solution is obtained with the Laplace transform and can be found in Hwang and Balluffi's article.[29]

The problem and solution simplify as the surface diffusion coefficient becomes infinitely larger than the grain boundary diffusion coefficient ($D_s \gg D_b$). When this condition is met, one can assume that the surface concentration does not vary with position and changes only with time. In effect, diffusion is so rapid that the concentration is the same at all values of y along the surface. The analytical solution for this scenario was adapted from an analogous heat transfer problem originally solved by Carslaw and Jaeger[32] and is shown below[33]

$$\frac{c_s}{c_0\ s'} = 1-2\sum_{n=1}^{\infty} \exp\left(-\theta_n^2 \frac{D_b t}{h^2}\right) \frac{\left(\theta_n^2+H^2\right)\sin\theta_n}{\left(\theta_n^2+H^2+H\right)\theta_n} \tag{9}$$

where θ_n is the nth root of

Table 1. List of Parameters Used in the Diffusion Model Along with Approximated Values

Parameter	Description	Value
C_0	Source concentration	4 at %
δ	GB width	3 nm
h	Mo thickness	680 nm
d_s	Grain width	50 nm
δ_s	Accumulation layer thickness	0.2 nm
D_b	GB diffusion coefficient	Fit to data
S'	Surface segregation factor	Fit to data

$$\theta \tan\theta = H \tag{10}$$

and H is a dimensionless quantity representing the ratio of grain boundary capacity to accumulation layer capacity

$$H=\frac{\delta h}{\delta_s d_s s'} \tag{11}$$

This fast surface diffusion approximation should be valid for the system used in this study based on experimental data of the amount of time it takes to reach saturation compared to the amount of time it takes Na to first appear. If surface diffusion were limiting, one would expect that it would take much longer for the surface to become saturated with Na. Additionally, when fitting the experimental data to the full Hwang–Balluffi solution, which includes surface diffusion, the optimized value of D_s is arbitrarily large (fit not shown), further validating the use of the Carslaw–Jaeger solution.

Table 1 summarizes all parameters used in the Carslaw–Jaeger solution along with estimations for their values. After accounting for the Mo microstructure, the only remaining unknown parameters are D_b, and s'. Because D_s is essentially infinite, it is no longer a parameter.

Equation 9 was fit to experimental data using a downhill simplex algorithm to minimize the residual sum of squares while varying D_b, and s'. Figure 6 shows fits of the XPS diffusion data from as-deposited SLG/Mo heated at 300, 350, and 400°C. Table 2 shows the optimized values for D_b and s' from these three heat treatments and also compares the as-deposited sample at 400°C to a sputter etched sample with a low amount of surface oxygen, also heated to 400°C.

The optimized values of D_b at 400°C for the as-deposited sample with high oxygen and sputter etched sample with low oxygen vary by only 50%. The difference between these two values of D_b is not significant given the precision of these measurements. Although the oxygen at grain boundaries plays a role in Na diffusion, sputter etching does not alter the amount of oxygen within the bulk of the film, and D_b remains unchanged. It has been demonstrated that Na diffusion is enhanced in Mo films with a greater bulk oxygen concentration,[16,34] and it is expected that the value of D_b would increase with the concentration of oxygen at the grain boundaries.

Conversely, the surface segregation factor, s', is expected to be dependent on surface properties, and its value for the sample with a large amount of surface oxygen is nearly nine times greater than the sample with a low amount of surface oxygen. Surface adsorbates have been shown to alter surface segregation of the diffusing species[35] and this effect could contribute to the observation that samples with more surface oxygen accumulate more Na. Furthermore, the surface segregation factor is known to depend on temperature[36] which

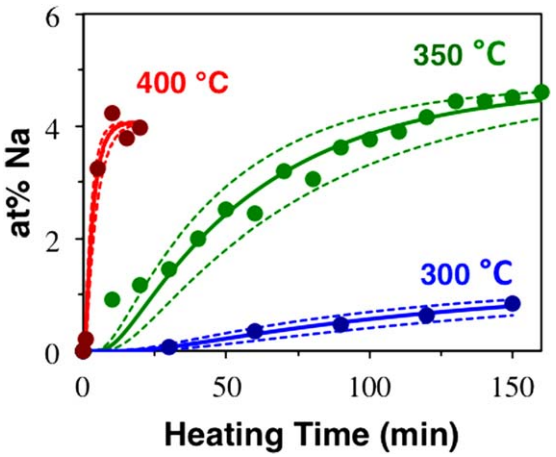

Figure 6. The Hwang–Balluffi model (solid line) fit to experimental data (circles) for as-deposited SLG/Mo samples after diffusion at 400, 350, and 300°C.

Dashed lines denote the model with ±25% of the optimized grain boundary diffusion coefficient. [Color figure can be viewed in the online issue, which is available at wileyonlinelibrary.com.]

can explain the increase in Na saturation concentration for heat treatments at 500°C and its decrease for the experiment performed at 300°C.

As expected the grain boundary diffusion coefficient increases with temperature. Typically the temperature dependence of a diffusion coefficient follows an Arrhenius type relation

$$D(T) = D_0 \exp\left(\frac{E_a}{RT}\right) \tag{12}$$

where D_0 is the pre-exponential factor and E_a is the apparent activation energy for grain boundary diffusion. Figure 7 plots the natural logarithm of D_b against the inverse of temperature. The measurement at 400°C was performed twice, and both data points are shown in the figure. This plot is linear confirming that Na diffusion through Mo has an Arrhenius type dependency on temperature. The slope resulted in an estimate of the apparent activation energy of 117 kJ/mol. As a rule of thumb for grain boundary diffusion in metals, Gupta suggests that the activation energy in cal/mol should be 17–25 times melting temperature of the diffusion matrix in Kelvin.[37] For grain boundary diffusion in Mo, this gives an estimated activation energy of roughly 206–303 kJ/mol. Because activation energy measured for this system is so much lower than expected, it is likely that the transport of Na in Mo may not follow a standard mechanism for grain boundary diffusion. Arnoldy reports an activation energy of the Mo—O bond breaking during the reduction of MoO_3 to

Table 2. Optimized Values of D_b and s' for Various Temperatures and Surface Oxygen Concentrations

Treatment	Initial O (at %)	T (°C)	D_b (CM^2/s)	s'
Sputter etched	11	400	7.8×10^{-12}	0.12
None	53	400	12×10^{-12}	1.02
None	44	350	6.5×10^{-13}	1.18
None	54	300	2.9×10^{-13}	0.31

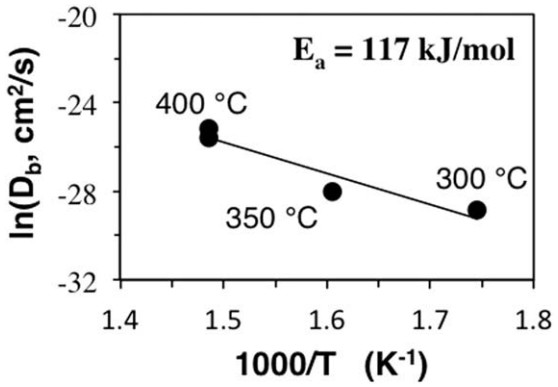

Figure 7. Arrhenius plot for the grain boundary diffusion coefficient.

be 120 kJ/mol,[38] which is in good agreement with activation energy from Figure 7, suggesting that the Mo—O bond is involved with the diffusion of Na.

Figure 8 shows an Ellingham diagram depicting the Gibbs free energy of formation for Na_2O, MoO_3, and MoO_2 calculated using published data.[39] Na_2O is more stable than both Mo oxides suggesting that Na is thermodynamically capable of disrupting Mo—O bonds at the grain boundary.

Conclusions

By selectively adding or removing oxygen from the surface of Mo coated SLG, we show a linear relationship between the surface oxygen concentration and the amount of Na that ultimately accumulates. We modeled the diffusion and accumulation of Na using the Hwang–Balluffi method with a fast-surface diffusion approximation adapted from Carslaw and Jaeger. Fitting the solution of this model to experimental data revealed that the surface segregation parameter is the only parameter that significantly varies with oxygen content. Surface oxygen can affect the amount of surface segregation and thus the overall saturation

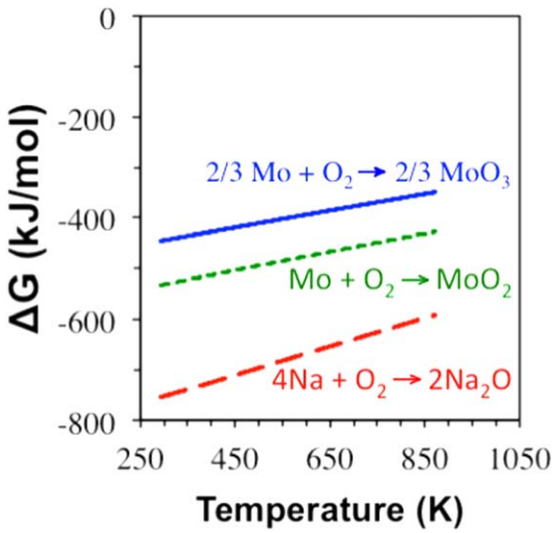

Figure 8. Ellingham diagram depicting Gibbs free energy of formation for Na_2O, MoO_2, and MoO_3.

[Color figure can be viewed in the online issue, which is available at wileyonlinelibrary.com.]

concentration of Na. We also calculate an apparent activation energy for the diffusion of Na through Mo grain boundaries. Our reported value of 117 kJ/mol is in good agreement with the activation energy for breaking the Mo—O bond in MoO_3, suggesting Na—O bonds partially disrupt Mo—O bonds as Na diffuses through the grain boundary. This result along with the increased saturation concentration of Na on samples with large amounts of surface oxygen show that oxygen provides a chemical driving force for the diffusion of Na through Mo.

Acknowledgments

The authors thank K. Hart for his contribution of making the Mo films used in this study and Dr. S. Rykov for his assistance in maintaining the XPS system. The authors also thank Dr. A. Rockett and P. Tsai for performing SIMS and AES measurements. This work is funded by the US Department of Energy FPACE program under contract number DE-EE5402.This report was prepared as an account of work sponsored by an agency of the United States Government. Neither the United States Government nor any agency thereof, nor any of their employees, makes any warranty, express or implied, or assumes any legal liability or responsibility for the accuracy, completeness, or usefulness of any information, apparatus, product, or process disclosed, or represents that its use would not infringe privately owned rights. Reference herein to any specific commercial product, process, or service by trade name, trademark, manufacturer, or otherwise does not necessarily constitute or imply its endorsement, recommendation, or favoring by the United States Government or any agency thereof. The view and opinions of authors expressed herein do not necessarily state or reflect those of the United States Government or any agency thereof.

Literature Cited

1. Niki S, Contreras M, Repins I, Powalla M, Kushiya K, Ishizuka S, Matsubara K. CIGS absorbers and processes. *Prog Photovoltaics Res Appl*. 2010;18(6):453–466.
2. Jackson P, Hariskos D, Lotter E, Paetel S, Wuerz R, Menner R, Wischmann W, Powalla M. New world record efficiency for Cu(In,Ga)Se_2 thin-film solar cells beyond 20%. *Prog Photovoltaics Res Appl*. 2011;19(7):894–897.
3. Chirilă A, Reinhard P, Pianezzi F, Bloesch P, Uhl AR, Fella C, Kranz L, Keller D, Gretener C, Hagendorfer H, Jaeger D, Erni R, Nishiwaki S, Buecheler S, Tiwari AN. Potassium-induced surface modification of Cu(In,Ga)Se_2 thin films for high-efficiency solar cells. *Nat Mater*. 2013;12(12):1107–1111.
4. Igalson M, Kubiaczyk A, Zabierowski P, Bodegård M, Granath K. Electrical characterization of ZnO/CdS/Cu(In,Ga)Se_2 devices with controlled sodium content. *Thin Solid Films*. 2001;387:225–227.
5. Rudmann D, da Cunha AF, Kaelin M, Kurdesau F, Zogg H, Tiwari AN, Bilger G. Efficiency enhancement of Cu(In,Ga)Se_2 solar cells due to post-deposition Na incorporation. *Appl Phys Lett*. 2004;84(7):1129–1131.
6. Ård M, Granath K, Stolt L. Growth of Cu(In, Ga)Se_2 thin films by coevaporation using alkaline precursors. *Thin Solid Films*. 2000;361–362:9–16.
7. Yun JH, Kim KH, Kim MS, Ahn BT, Ahn SJ, Lee JC, Yoon KH. Fabrication of CIGS solar cells with a Na-doped Mo layer on a Na-free substrate. *Thin Solid Films*. 2007;515(15):5876–5879.
8. Lammer M, Kniese R, Powalla M. In-line deposited Cu(In,Ga)Se_2 solar cells: influence of deposition temperature and Na co-evaporation on carrier collection. *Thin Solid Films*. 2004;451–452:175–178.
9. Ye S, Tan X, Jiang M, Fan B, Tang K, Zhuang S. Impact of different Na-incorporating methods on Cu(In,Ga)Se_2 thin film solar cells with a low-Na substrate. *Appl Opt*. 2010;49(9):1662–1665.
10. Caballero R, Kaufmann CA, Eisenbarth T, Unold T, Schorr S, Hesse R, Klenk R, Schock HW. The effect of NaF precursors on low temperature growth of CIGS thin film solar cells on polyimide substrates. *Phys Status Solidi (a)*. 2009;206(5):1049–1053.
11. Tan XH, Ye SL, Fan B, Tang K, Liu X. Effects of Na incorporated at different periods of deposition on Cu(In,Ga)Se_2 films. *Appl Opt*. 2010;49(16):3071–3074.
12. Rudmann D, Breḿaud D, Zogg H, Tiwari AN. Na incorporation into Cu(In,Ga)Se_2 for high-efficiency flexible solar cells on polymer foils. *J Appl Phys*. 2005;97(8):084903.
13. Kronik L, Mishori B, Fefer E, Shapira Y, Riedl W. Quality control and characterization of Cu(In,Ga)Se_2-based thin-film solar cells by surface photovoltage spectroscopy. *Sol Energy Mater Sol Cells*. 1998;51(1):21–34.
14. Granath K, Stolt L, Bodegård M, Rockett A, Schroeder DJ. Sodium in sputtered Mo back contacts for Cu(In,Ga)Se_2 devices: incorporation, diffusion, and relationship to oxygen. In: *Proceedings of 14th European Photovoltaic Solar Energy Conference*. Barcelona, Spain, 1997:1278–1282.
15. Rockett A, Bodegård M, Granathc K, Stolt L. Na incorporation and diffusion in $CuIn_{1-x}Ga_xSe_2$. In: *Proceedings of 25th IEEE Photovoltaic Specialists Conference*. Washington, D.C., 1996:985–987.
16. Yoon J-H, Seong T-Y, Jeong J-h. Effect of a Mo back contact on Na diffusion in CIGS thin film solar cells. *Prog Photovoltaics Res Appl*. 2013;21(1):58–63.
17. Yoon J-H, Cho S, Kim WM, Park J-K, Baik Y-J, Lee TS, Seong T-Y, Jeong J-h. Optical analysis of the microstructure of a Mo back contact for Cu(In,Ga)Se_2 solar cells and its effects on Mo film properties and Na diffusivity. *Sol Energy Mater Sol Cells*. 2011;95(11):2959–2964.
18. Al-Thani H, Hasoon F, Young M, Asher S, Alleman JL, Al-Jassim MM, Williamson DL. The effect of Mo back contact on Na out-diffusion and device performance of Mo/Cu(In, Ga)Se_2/CdS/ZnO solar cells. In: *Record of 29th IEEE Photovoltaic Specialists Conference*. New Orleans, 2002:720–723.
19. Bommersbach P, Arzel L, Tomassini M, Gautron E, Leyder C, Urien M, Dupuy D, Barreau N. Influence of Mo back contact porosity on co-evaporated Cu (In,Ga)Se_2 thin film properties and related solar cell. *Prog Photovoltaics Res Appl*. 2013;21(3):332–343.
20. Scofield JH, Asher S, Albin D, Tuttle M, Contreras M, Niles D, Reedy R, Tennant A, Noufi R. Sodium diffusion, selenization, and microstructural effects associated with various molybdenum back contact layers for CIS-based solar cells. In: *Proceedings of 1st IEEE World Conference on Photovoltaic Energy Conversion, Vol. 1*. 1994;1:164–167.
21. Subramanian PR. Mo-Na (molybdenum-sodium). In: Massalski TB, editor. *Binary Allow Phase Diagrams*, 2nd ed. Materials Park: ASM International, 1990:2631–2633.
22. Assmann L, Bernede JC, Drici A, Amory C, Halgand E, Morsli M. Study of the Mo thin films and Mo/CIGS interface properties. *Appl Surf Sci*. 2005;246(1–5):159–166.
23. Zellner MB, Birkmire RW, Eser E, Shafarman WN, Chen JG. Determination of activation barriers for the diffusion of sodium through CIGS thin-film solar cells. *Prog Photovoltaics Res Appl*. 2003;11(8):543–548.
24. Salomé PMP, Fjallstrom V, Hultqvist A, Szaniawski P, Zimmermann U, Edoff M. The effect of Mo back contact ageing on Cu(In,Ga)Se2 thin-film solar cells. *Prog Photovoltaics Res Appl*. 2013;22(1):83–89.
25. Yamaguchi T, Miyagawa R. Effects of Oxygen on the properties of sputtered molybdenum thin films. *Jpn J Appl Phys*. 1991;30(9A):2069–2073.
26. Rockett A, Granath K, Asher S, Al Jassim AA, Hasoon F, Matson R, Basol B, Kapur V, Britt JS, Gillespie T, Marshall C. Na incorporation in Mo and CuInSe2 from production processes. *Sol Energy Mater Sol Cells*. 1999;59(3):255–264.
27. Srivastava SC, Seigle LL. Solubility and thermodynamic properties of oxygen in solid molybdenum. *Metall Trans*. 1974;5(1):49–52.
28. Gupta D, Ho P. Diffusion processes in thin films. *Thin Solid Films*. 1980;72:399–418.
29. Hwang JCM, Balluffi RW. Measurement of grain-boundary diffusion at low temperatures by the surface accumulation method. *I. Method and analysis. J Appl Phys*. 1979;50(3):1339–1348.
30. Lin J, Budhani R, Bunshah R. Effects of substrate bias on the resistivity and microstructure of molybdenum and molybdenum silicide films. *Thin Solid Films*. 1987;153(1–3):359–368.
31. Hwang JCM, Pan JD, Balluffi RW. Measurement of grain-boundary diffusion at low temperature by the surface-accumulation

method. *II. Results for gold-silver system. J Appl Phys.* 1979; 50(3):1349–1359.
32. Carslaw HS, Jaeger JC. *Conduction of Heat in Solids*. Oxford, UK: Clarendon Press, 1959:121–126.
33. Kaur I, Mishin Y, Gust W. *Fundamentals of Grain and Interphase Boundary Diffusion*, 3rd ed. New York, NY: Wiley, 1995:287–289.
34. Palm J, Probst V, Brummer A, Stetter W, Tölle R, Niesen TP, Visbeck S, Hernandez O, Wendl M, Vogt H, Calwer H, Freienstein B, Karg F. CIS module pilot processing applying concurrent rapid selenization and sulfurization of large area thin film precursors. *Thin Solid Films.* 2003;431–432(03):514–522.
35. Hwang JCM, Ho PS, Balluffi RW. Effect of surface condition on diffusion in thin films at low temperatures. *Appl Phys Lett*. 1978; 33(5):458–461.
36. Swaminarayan S, Srolovitz D. Surface segregation in thin films. *Acta Mater*. 1996;44(5):2067–2072.
37. Gupta D. Some formal aspects of diffusion: bulk solids and thin films. In: Gupta D, Ho PS, editors. *Diffusion Phenomena in Thin Films and Microelectronic Materials*. Park Ridge, NJ: Noyes Publications, 1988:44.
38. Arnoldy P, Jonge D, Moulijn JA. Temperature-programmed reduction of MoO_3 and MoO_2. *J Phys Chem.* 1985;89(21):4517–4526.
39. Knacke O, Kubaschewski O, Hesselmann K. *Thermochemical Properties of Inorganic Substances*, Vol. I & II, 2nd ed. Berlin: Springer-Verlag, 1991.

Manuscript received Oct. 22, 2013, and revision received Jan. 18, 2014.